International Journal of Wavelets, Multiresolution
and Information Processing
Vol. 9, No. 2 (2011) 211–225

DOI: 10.1142/S0219691311004055

World Scientific
www.worldscientific.com

FEATURE EXTRACTION OF SEWER PIPE DEFECTS USING WAVELET TRANSFORM AND CO-OCCURRENCE MATRIX

MING-DER YANG

Department of Civil Engineering, National Chung Hsing University, 250 Kuo Kuang Rd., Taichung 402/Taiwan, R. O. C.
mdyang@dragon.nchu.edu.tw

TUNG-CHING SU*

Department of Construction Engineering, National Quemoy University, 1 University Rd., Kinmen 892/Taiwan, R. O. C.
spcyj@nqu.edu.tw

NANG-FEI PAN

Department of Civil Engineering, National Cheng Kung University, 1 University Rd., Tainan 701/Taiwan, R. O. C.
nfpan@mail.ncku.edu.tw

PEI LIU

Department of Transportation and Traffic Engineering and Management, Feng Chia University, 100 Wenhwa Rd. Taichung, 407/Taiwan, R. O. C.
peiliu@fcu.edu.tw

Received 24 April 2009
Revised 7 December 2010

In general, the sewer inspection usually employs a great number of CCTV images to discover sewer failures by human interpretation. A computer-aided program remains to be developed due to human's fatigue and subjectivity. To enhance the efficiency of sewer inspection, this paper attends to apply artificial intelligence to extract the failure features of the sewer systems that is demonstrated on the sewer system in the eastern Taichung City, Taiwan. Wavelet transform and gray-level co-occurrence matrix, which have been widely applied in many texture analyses, are adopted in this research to generate extracted features, which are the most valuable information in pattern recognition of failures on CCTV images. Wavelet transform is capable of dividing an image into

*Corresponding author.

four sub-images including approximation sub-image, horizontal detail sub-image, vertical detail sub-image, and diagonal detail sub-image. The co-occurrence matrices of horizontal orientation, vertical orientation, and 45° and 135° orientations, respectively, were calculated for the horizontal, vertical, and diagonal detail sub-images. Subsequently, the features including angular second moment, entropy, contrast, homogeneity, dissimilarity, correlation, and cluster tendency, can be obtained from the co-occurrence matrices. However, redundant features either decrease the accuracy of texture description or increase the difficulty of pattern recognition. Thus, the correlations of the features are estimated to search the appropriate feature sets according to the correlation coefficients between the features. In addition, a discriminant analysis was used to evaluate the discriminability of the features for the pipe failure defection, and entropy, correlation, and cluster tendency were found to be the best features based on the discriminant accuracy through an error matrix analysis.

Keywords: Feature extraction; wavelet transform (WT); gray-level co-occurrence matrix; CCTV images.

AMS Subject Classification: 22E46, 53C35, 57S20

1. Introduction

In Taiwan, the percentage of population served by the infrastructures of sewer is below 22.10% that has driven a great attention from the government and environmental societies. To rise up the sewer-serving percentage, the Construction and Planning Agency of Taiwan has been making great efforts to establish the sewer construction all over the island. After a new sewer construction, sewer inspection is executed prior to house-connection.[1]

Sewer inspection involves routines inspection, detailed inspection, and special inspection.[2] Routines inspection is to inspect sewer pipes roughly, so its inspection accuracy is usually less than detailed inspection. Special inspection is to implement an inspection for some specific events. Nowadays, engineers apply various tools and technologies such as closed circuit television (CCTV) cameras mounted on robots, ground piercing radar (GPR), sonar and infrared thermograph, to sewage inspection.[3–7] With a commercial availability, CCTV is considered as the most popular image source for sewer inspection. CCTV camera is usually mounted on robot moving inside sewer pipes from a manhole and remotely-controlled outside to acquire the images of inner pipe.[5] Mobile CCTV system has many advantages, such as fewer inspectors needed, more safety-ensured to inspectors, and more detailed data of distance and slope possibly recorded.[2] The Water Research Centre (WRC) in UK categorizes major sewer pipe defects appearing on CCTV images into 10 classes, including open joint, displaced joint, crack, fracture, broken pipe, hole, collapse, spalling, wear, and deformation.[8]

In general, the sewer inspection usually employs a great number of CCTV images to discover sewer failures by human interpretation. However, human interpretation is not suitable for detecting a great number of CCTV images due to human's fatigue, subjectivity, and cost.[9] To overcome these limitations, the artificial intelligence has been variously employed in diagnosis of sewer pipe defects. Moreover, some

computer-aided systems have been developed to replace human interpretation for detecting pipe defects on a great number of CCTV images.[6,9,10]

In common, color and texture are the two typical features used to describe an object. For interpretation of sewer pipe defects, texture is more critical compared to color. Some efficient approaches had been applied in extraction of textural features.[11] Recently, a wavelet-based perceptual image model coupled with Human Visual System to produce high quality images was developed for the compression of color images,[12] and a wavelet-based model coupled with novel biologically-inspired model was established for extracting features of faces from face images.[13] Wavelet descriptors are concluded insensitive to individual shape variations and better than Fourier descriptors in shape representation for handprinted characters.[14] A combination of wavelet transform (WT) and co-occurrence matrices was used to extract the co-occurrence features of defective textile fabrics and demonstrated being powerful in detecting defects.[15] This research adopted wavelet transform and co-occurrence matrices to extract the feature of pipe defects on CCTV inspection images.

2. Experimental Equipments

The sewer system in the 9th district of Taichung city, the largest city in the central Taiwan, consists of ten subsystems, subsystem A through J. Figure 1 is the layout of the sewer system. In 2002, the CCTV inspection work provides engineers with 1,101 frames of CCTV images for diagnosing the sewer pipe defects. To acquire the enormous amount of CCTV inspection images, the hardware and software for sewer pipe failure detection are briefly introduced as follows:

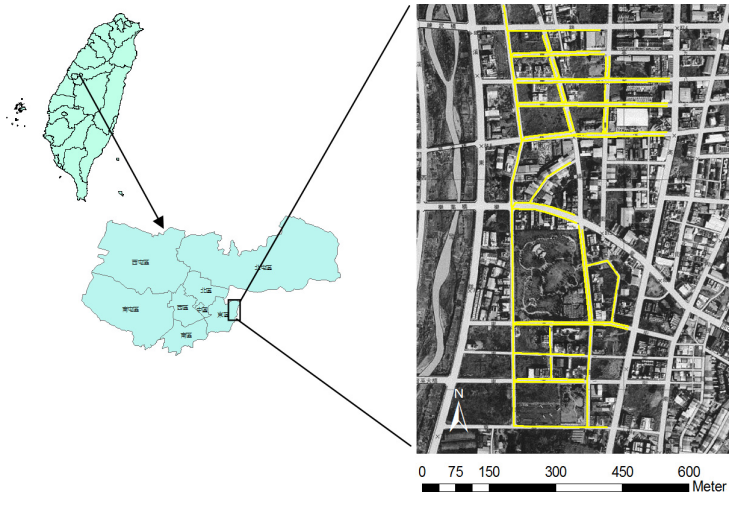

Fig. 1. Layout of the sewer system in the 9th district of Taichung city.

2.1. *Mobile closed circuit television (CCTV) system*

A mobile CCTV system for defect inspection of inner pipe consists of a camera with self-lighting and propelled monitoring equipment, connected by multicore cable used for power supply and inspection modules. The cable, with a maximum length of 250 m, wound around a drum equipped with a mechanism also can be used to position the pipe defects with other accessories of a video-recorder, a computer system for recording, and a video-printer or ordinary printer, which are usually mounted in a vehicle above the ground.

Mobile CCTV can be applied to sewer inspection within a pipe with a cross-section ranging from 100 mm to 1,500 mm. The operation of mobile CCTV is first to put the camera mounted on a robot, which moves between the manholes and is controlled by the equipments in the vehicle on the ground. While the robot moves forward, the inner pipe is monitored and recorded by the camera and the video-recorder, respectively. If a pipe defect is detected, the camera can stop in time to make precise examination and to document details. However, sometimes pipe defects are not easily detected due to the original conditions of camera itself including its available angle of lenses, focal length (zoom), light, and resolution. Thus, the cameras used for inspection of inner pipe are suggested to be equipped with wide-angle lenses, adjustable diaphragm, variable focal length, and high resolution sensor. Furthermore, the brightness and sharpness of CCTV images, either color or black-and-white, should be enabled to be adjusted automatically or manually from the control vehicle.[2]

2.2. *Software and hardware for image processing*

In this research, Matlab 6.5 was used to program the algorithm codes of extracting pipe defect features due to its friendly environment and good performance in both image processing and matrix computation. A personal computer equipped with AMD1600+ CPU, 256 MB RAM, and 40 GB disk, was used to store the CCTV inspection images and to implement image processing.

3. Methodology

3.1. *Wavelet transform*

Wavelet transform (WT) is a linear transform developed from Fourier transform. However, unlike Fourier transform whose basis functions are sinusoids, wavelet transform is based on small waves, so-called wavelet, of varying frequency and limited duration so as to obtain better resolutions along frequency scale.[16–18] Although WT has been known for many years, it was not applied to image processing until Daubechies, who provided the discretization of WT, and Mallat, who established the connection between WT and the multiresolution theory. Moreover, signals in multiresolution represented by WT is believed to enable extraction of more powerful features than the signal scale case.[15,19–21]

The sets of scaling and wavelet functions are defined as:

scaling function

$$\varphi_{a,b}(x) = 2^{\frac{a}{2}}\varphi(2^a x - b), \tag{3.1}$$

wavelet function

$$\psi_{a,b}(x) = 2^{\frac{a}{2}}\psi(2^a x - b), \tag{3.2}$$

for all $a, b \in Z$. Z is the set of integers. The scale parameter a controls stretch or compression of the mother wavelet function; the translation parameter b is an offset along the time axis; $2^{0.5a}$ controls its height or amplitude.[17,22] For multiresolution analysis, it is required that subspaces S_a containing high resolution functions must contain all lower resolution functions.[15] The expansion functions of subspace S_a are expressed as a weighted sum of those of subspace S_{a+1}. Thus,

$$\varphi_{a,b}(x) = \sum_n h_\varphi(n)\varphi_{a+1,n}(x), \tag{3.3}$$

where $h_\varphi(n)$ are called scaling function coefficients. Substituting Eq. (3.1) for $\varphi_{a+1,n}(x)$, Eq. (3.3) becomes

$$\varphi_{a,b}(x) = \sum_n h_\varphi(n)2^{\frac{a+1}{2}}\varphi(2^{a+1}x - n). \tag{3.4}$$

If both a and b are set to 0, Eq. (3.4) becomes

$$\varphi_{0,0}(x) = \varphi(x) = \sum_n h_\varphi(n)2^{\frac{1}{2}}\varphi(2x - n). \tag{3.5}$$

If x is scaled by 2^a, translated by b, and n is let as $m - 2b$, it is given as:

$$\begin{aligned}\varphi(2^a x - b) &= \sum_n h_\varphi(n)2^{\frac{1}{2}}\varphi(2(2^a x - b) - n) \\ &= \sum_m h_\varphi(m - 2b)2^{\frac{1}{2}}\varphi(2^{a+1}x - m).\end{aligned} \tag{3.6}$$

An analogous result for wavelet functions is shown as:

$$\psi(2^a x - b) = \sum_m h_\psi(m - 2b)2^{\frac{1}{2}}\varphi(2^{a+1}x - m). \tag{3.7}$$

Obviously a CCTV image can be regarded as the change of discrete signal along a two-dimensional (2D) scale. Hence, a 2D discrete WT (DWT) had been proved to be useful for signal or image processing and pattern recognition.[23,24] The fast wavelet transform was considered as a computationally efficient implementation of

the DWT was defined as:[17]

$$W_\varphi(a_0, b) = \frac{1}{\sqrt{M}} \sum_x f(x)\varphi_{a_0,b}(x), \tag{3.8}$$

$$W_\psi(a, b) = \frac{1}{\sqrt{M}} \sum_x f(x)\psi_{a,b}(x), \tag{3.9}$$

for $a \geq a_0$ and

$$f(x) = \frac{1}{\sqrt{M}} \sum_b W_\varphi(a_0, b)\varphi_{a_0,b}(x) + \frac{1}{\sqrt{M}} \sum_{a=a_0}^{\infty} \sum_b W_\psi(a, b)\psi_{a,b}(x), \tag{3.10}$$

where $f(x), \varphi_{a_0}, b(x)$, and $\psi_a, b(x)$ are the functions of the discrete variables $x = 0, 1, 2, \ldots, M-1$. Considering $\psi_a, b(x)$ in Eq. (3.9) substituted by Eq. (3.2), we get

$$W_\psi(a, b) = \frac{1}{\sqrt{M}} \sum_x f(x)2^{\frac{a}{2}}\psi(2^a x - b). \tag{3.11}$$

Replacing $\psi(2^a x - b)$ with the right-hand side of Eq. (3.7), Eq. (3.11) becomes

$$W_\psi(a, b) = \frac{1}{\sqrt{M}} \sum_x f(x)2^{\frac{a}{2}} \sum_m h_\psi(m - 2b)2^{\frac{1}{2}}\varphi(2^{a+1}x - m). \tag{3.12}$$

It also can be rewritten as

$$W_\psi(a, b) = \sum_m h_\psi(m - 2b)\frac{1}{\sqrt{M}} \sum_x f(x)2^{\frac{a+1}{2}}\varphi(2^{a+1}x - m), \tag{3.13}$$

or

$$W_\psi(a, b) = \sum_m h_\psi(m - 2b)W_\varphi(a + 1, m). \tag{3.14}$$

Also, a similar derivation involving the DWT approximation coefficients is obtained as:

$$W_\varphi(a, b) = \sum_m h_\varphi(m - 2b)W_\varphi(a + 1, m). \tag{3.15}$$

$W_\varphi(a, b)$ and $W_\psi(a, b)$ are computed by convolving $W_\varphi(a + 1, b)$ with the time-reversed scaling and wavelet vectors, $h_\varphi(n)$ and $h_\psi(n)$. In other words, the original function, $W_\varphi(a + 1, b)$, is split into a low-pass (approximation component) corresponds to $W_\varphi(a, b)$, and a high-pass (detail component) corresponding to $W_\psi(a, b)$.

In multiresolution analysis (MRA), a scaling function is to create a series of approximation of a function or an image; additional functions, i.e. wavelet functions, are then used to encode the information difference between adjacent approximations.[17,25] CCTV images can be regarded as the change of discrete signal along a two-dimensional (2D) scale. Hence, a 2D discrete WT (DWT) was proved to be useful for signal or image processing and pattern recognition.[23–27] Through a decomposition of 2D discrete WT, which is implemented by consecutive low-pass (L) and high-pass (H) filtering through one-dimensional convolution, a CCTV inspection image $X(m, n)$ can be divided into an approximation image (LL) and three

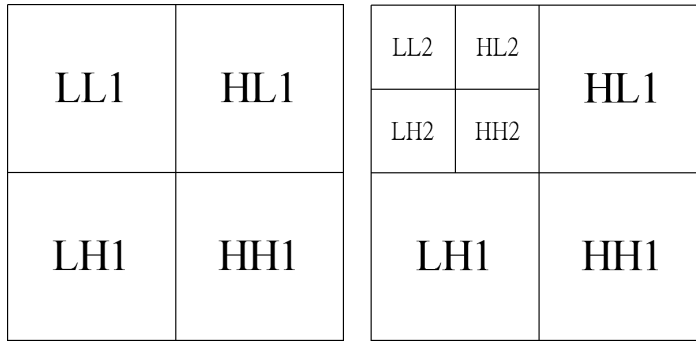

(a) 1-Level 2-DWT (b) 2-Level 2-DWT

Fig. 2. Illustration of image compression.

detail images in horizontal (HL), vertical (LH), and diagonal (HH) orientations (see Fig. 2(a)). At each recurring step of decomposition, the approximation image is split into a next level of approximation and detail images (see Fig. 2(b)). Until no more valuable information is obtained, the recurring step of decomposition for a CCTV image is terminated.

3.2. *Co-occurrence features*

A co-occurrence matrix is a square matrix in which each element M_ij in row (i) and column (j) directions records a relative occurrence frequency of a pair of pixels with the same gray level value separated by a certain pixel distance in one direction.[2,19] An example of a co-occurrence matrix computed by one pixel distance in row direction is shown in Fig. 3. The size of co-occurrence matrix depends on the range of the gray level values of the CCTV image. The element $M_1 1$ is recorded as 1 due to only one pair of gray level value "0" in the image separated by one pixel distance in row direction. Collecting the value for the co-occurrence matrix is

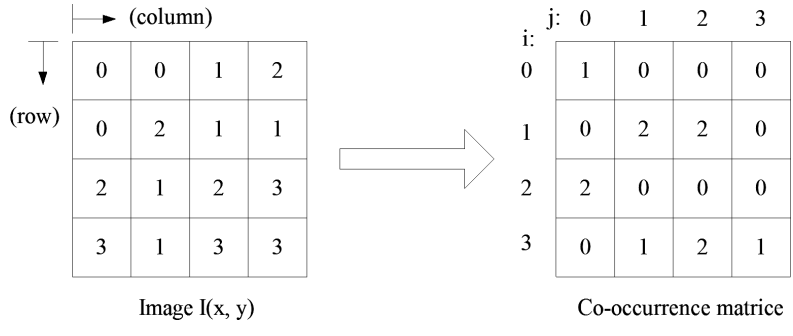

Fig. 3. Example of co-occurrence matrix computation.

extremely simple but time-consuming, if the image has 256 distinct levels of gray.[26] The means, μ_x and μ_y, and standard deviations, σ_x and σ_y, which have been widely used as descriptors for the image data, can be used for the co-occurrence matrices. Generally, distances of one pixel in the orientations of $0°, 90°, 45°$, and $135°$ are used to extract the co-occurrence features from the horizontal, vertical, and diagonal detail sub-images, respectively.[29] In other words, the co-occurrence features in four orientations can be extracted from a CCTV image for the pipe defect. The co-occurrence features in each orientation consist of angular second moment (ASM), entropy (ENT), contrast (CON), homogeneity (HOM), dissimilarity (DIS), correlation (COR), and cluster tendency (CLU), and can be calculated as follows:

$$\text{ENT} = \sum_{i=1}^{n}\sum_{j=1}^{n} P_{ij} \log P_{ij}, \tag{3.16}$$

$$\text{ASM} = \sum_{i=1}^{n}\sum_{j=1}^{n} P_{ij}^2, \tag{3.17}$$

$$\text{CON} = \sum_{i=1}^{n}\sum_{j=1}^{n} (i-j)^2 P_i j, \tag{3.18}$$

$$\text{HOM} = \sum_{i=1}^{n}\sum_{j=1}^{n} \frac{P_{ij}}{1+(i-j)^2}, \tag{3.19}$$

$$\text{COR} = \frac{\sum_{i=1}^{n}\sum_{j=1}^{n} (i \cdot j) P_{ij} - \mu_x \mu_y}{\sigma_x \sigma_y}, \tag{3.20}$$

$$\text{CLU} = \sum_{i=1}^{n}\sum_{j=1}^{n} (i - \mu_x + j - \mu_y)^2 \cdot P_{ij}, \tag{3.21}$$

$$\text{DIS} = \sum_{i=1}^{n}\sum_{j=1}^{n} |i-j| \, P_{ij}, \tag{3.22}$$

where

$$P_i j = \frac{M_{ij}}{\sum_{i=1}^{n}\sum_{j=1}^{n} M_{ij}}, \tag{3.23}$$

$$\mu_x = \sum_{i=1}^{n}\sum_{j=1}^{n} i \cdot P_{ij}, \tag{3.24}$$

$$\mu_y = \sum_{i=1}^{n}\sum_{j=1}^{n} j \cdot P_{ij}, \tag{3.25}$$

$$\sigma_x = \sqrt{\sum_{i=1}^{n}\sum_{j=1}^{n}(i-\mu_x)^2 \cdot P_{ij}}, \tag{3.26}$$

$$\sigma_y = \sqrt{\sum_{i=1}^{n}\sum_{j=1}^{n}(j-\mu_y)^2 \cdot P_{ij}}. \tag{3.27}$$

4. Results and Discussions

According to the diagnosis result, most of the detected pipe defects were found within system G which comprises 291 frames of CCTV. A statistics for the 291 CCTV images reveals that open joint, crack, broken pipe, and fracture are the major pipe defects, and appears on 107, 112, 16, and 56, respectively, frames of CCTV images. Figure 4 shows the typical CCTV images of the four pipe defects collected from system G.

4.1. *Texture analysis*

The averages of the co-occurrence features in the four orientations were respectively computed to describe the textures of the pipe defects. Tables 1–4 present

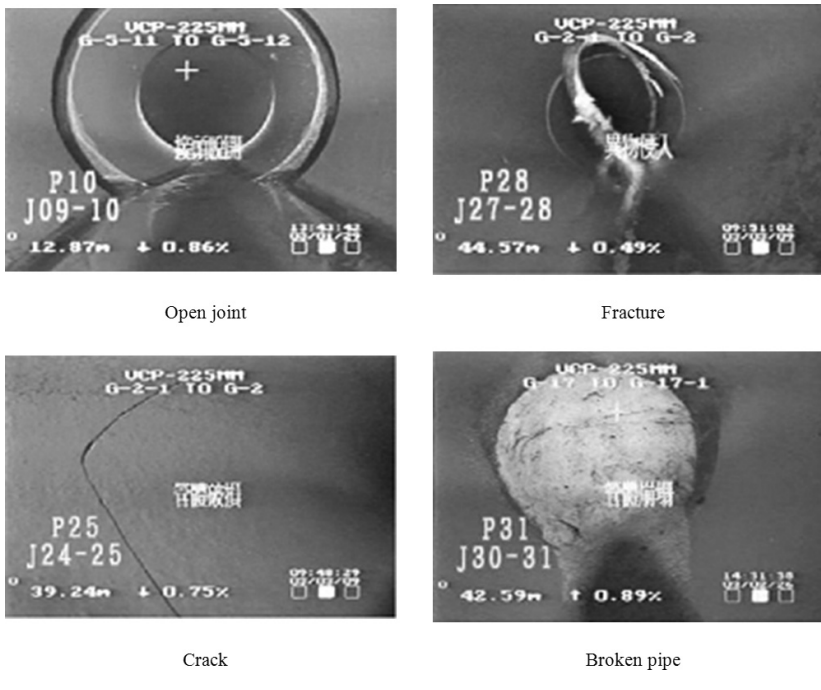

Fig. 4. CCTV image examples.

Table 1. Co-occurrence features in the orientation of 0°.

	Open joint	Fracture	Crack	Broken pipe
ASM	0.041	0.011	0.016	0.018
CON	219.739	343.183	285.528	378.26
HOM	0.423	0.258	0.3	0.299
ENT	2.016	2.495	2.241	2.419
DIS	6.081	8.771	6.953	9.287
COR	0.641	0.547	0.6	0.528
CLU	996.304	1173.165	725.077	1200.021

Table 2. Co-occurrence features in the orientation of 90°.

	Open joint	Fracture	Crack	Broken pipe
ASM	0.032	0.021	0.025	0.018
CON	338.008	437.972	301.804	409.582
HOM	0.384	0.304	0.34	0.295
ENT	2.21	2.368	2.141	2.454
DIS	7.91	9.574	6.917	9.655
COR	0.612	0.565	0.584	0.6
CLU	996.304	1173.165	725.077	1200.021

Table 3. Co-occurrence features in the orientation of 45°.

	Open joint	Fracture	Crack	Broken pipe
ASM	0.048	0.012	0.014	0.013
CON	302.997	489.327	370.482	484.55
HOM	0.394	0.239	0.263	0.251
ENT	2.054	2.497	2.301	2.514
DIS	7.229	10.636	8.456	10.871
COR	0.399	0.304	0.351	0.324
CLU	711.108	894.65	791.902	948.444

Table 4. Co-occurrence features in the orientation of 135°.

	Open joint	Fracture	Crack	Broken pipe
ASM	0.035	0.015	0.016	0.014
CON	423.872	555.004	403.423	596.865
HOM	0.363	0.254	0.284	0.253
ENT	2.169	2.455	2.254	2.518
DIS	8.821	11.129	8.523	11.783
COR	0.393	0.345	0.398	0.319
CLU	969.106	1126.746	953.434	1155.508

the computed co-occurrence features in the orientations of 0°, 90°, 45°, and 135°, respectively. Obviously, the values of ASM and HOM of open joint are larger than the others that means open joint having more homogenized texture relative to the other pipe defects. Also, the values of ENT of broken pipe are mostly larger than those of the other pipe defects. Thus, CCTV images of broken pipe usually have

a display of complex texture. For all four pipe defects, the values of COR in the orientations of 0° and 90° are larger than those in the orientations of 45° and 135°. It demonstrates that the correlations of detail images in the horizontal or vertical orientations are better than those in the diagonal orientation. In this paper, the averages of ENT, ASM, CON, HOM, COR, CLU, and DIS in the four orientations were used to represent the textural features of the pipe defect patterns.

4.2. *Correlation test of the co-occurrence features*

Even though the texture of a pipe defect could be described by ASM, CON, HOM, ENT, DIS, COR, and CLU, redundant features increase the difficulty of pattern recognition with no accuracy improvement of texture description. To search the appropriate feature sets, a correlation test shown as Table 5 was done for the seven co-occurrence features extracted from the 291 CCTV images. It is found that CLU vs. COR has a least correlation coefficient, −0.188. All of the correlation coefficients of ASM vs. CON, CON vs. HOM, ASM vs. COR, CON vs. COR, HOM vs. COR, ENT vs. COR, ASM vs. CLU, HOM vs. CLU, and ENT vs. CLU, are less than 0.5. In conclusion of the correlation test, (ASM, COR, CLU), (HOM, COR, CLU), and (ENT, COR, CLU) are considered as the candidate feature vectors due to low correlation coefficients.

4.3. *Discriminant analysis of the textural features*

A discriminant analysis available in the SPSS 13.0 for Windows software was used to evaluate the discriminability of the obtained textural features. Tables 6–10 show the discriminant analysis results based on ASM, HOM, ENT, COR, and CLU, respectively. Each discriminant analysis result lists the producer's and user's accuracies. The procedure's accuracies resulted from dividing the number of correctly classified pipe defect patterns in each category (on the major diagonal) by the number of training set pipe defect patterns used for that category (the column total) so to indicate how well the training set pipe defect patterns were classified. The user's accuracies were computed by dividing the number of correctly classified pipe defect patterns in each category by the total number of pipe defect patterns that were classified in that category (the row total) in order to measure commission error.

Table 5. Correlation matrix of the co-occurrence features.

	ASM	CON	HOM	ENT	DIS	COR	CLU
ASM	1.000	**−0.324**	0.945	−0.850	−0.556	**0.250**	**−0.242**
CON		1.000	**−0.423**	0.501	0.869	**−0.445**	0.943
HOM			1.000	−0.948	−0.701	**0.390**	**−0.311**
ENT				1.000	0.824	**−0.480**	**0.363**
DIS					1.000	−0.565	0.746
COR						1.000	**−0.188**
CLU							1.000

Table 6. Discriminant analysis based on ASM.

	Predicted sewer defect membership				
Original	Open joint	Cracks	Broken pipe	Fractures	Column total
Open joint	23	17	3	14	57
Cracks	77	89	13	36	215
Broken pipe	0	0	0	0	0
Fractures	7	6	0	6	19
Raw total	107	112	16	56	291
Producer's accuracy (%)		User's accuracy (%)		Overall accuracy = 40.5%	
Open joint	21.5	Open joint	40.3		
Cracks	79.5	Cracks	41.4		
Broken pipe	0.0	Broken pipe	100.0		
Fractures	10.7	Fractures	31.6		

Table 7. Discriminant analysis based on HOM.

	Predicted sewer defect membership				
Original	Open joint	Cracks	Broken pipe	Fractures	Column total
Open joint	58	57	3	21	139
Cracks	48	53	11	35	147
Broken pipe	0	0	2	0	2
Fractures	1	2	0	0	3
Raw total	107	112	16	56	291
Producer's accuracy (%)		User's accuracy (%)		Overall accuracy = 38.8%	
Open joint	54.2	Open joint	41.7		
Cracks	47.3	Cracks	36.1		
Broken pipe	12.5	Broken pipe	100.0		
Fractures	0.0	Fractures	0.0		

Table 8. Discriminant analysis based on ENT.

	Predicted sewer defect membership				
Original	Open joint	Cracks	Broken pipe	Fractures	Column total
Open joint	74	55	6	29	164
Cracks	31	55	5	22	113
Broken pipe	0	1	4	3	8
Fractures	2	1	1	2	6
Raw total	107	112	16	56	291
Producer's accuracy (%)		User's accuracy (%)		Overall accuracy = 46.4%	
Open joint	69.2	Open joint	45.1		
Cracks	49.1	Cracks	48.7		
Broken pipe	25.0	Broken pipe	50.0		
Fractures	3.6	Fractures	33.3		

Table 9. Discriminant analysis based on COR.

	Predicted sewer defect membership				
Original	Open joint	Cracks	Broken pipe	Fractures	Column total
Open joint	69	65	2	22	158
Cracks	35	41	6	26	108
Broken pipe	0	1	5	3	9
Fractures	3	5	3	5	16
Raw total	107	112	16	56	291
Producer's accuracy (%)		User's accuracy (%)		Overall accuracy = 41.2%	
Open joint	64.5	Open joint	43.7		
Cracks	36.6	Cracks	38.0		
Broken pipe	31.3	Broken pipe	55.6		
Fractures	8.9	Fractures	31.3		

Table 10. Discriminant analysis based on CLU.

	Predicted sewer defect membership				
Original	Open joint	Cracks	Broken pipe	Fractures	Column total
Open joint	71	40	7	39	157
Cracks	35	71	6	16	128
Broken pipe	1	1	2	1	5
Fractures	0	0	1	0	1
Raw total	107	112	16	56	291
Producer's accuracy (%)		User's accuracy (%)		Overall accuracy = 49.5%	
Open joint	66.4	Open joint	45.2		
Cracks	63.4	Cracks	55.5		
Broken pipe	12.5	Broken pipe	40.0		
Fractures	0.0	Fractures	0.0		

Tables 6–10 show that the pipe defects with more training patterns, such as open joint or cracks, have the better producer's accuracy. On the contrary, those with the less training patterns, such as broken pipe or fractures, have the better user's accuracies. Both of the user's accuracies of broken pipe in Tables 6 and 7 are 100%; however, only two of its 16 patterns were correctly classified in Table 7. Even no pipe defect patterns were classified into broken pipe in Table 6. Among the textural features, the obtained overall accuracy based on CLU is the best (see Table 10). Most of the patterns of open joint (71 of 107) and cracks (71 of 112) were correctly classified. Considering the result of the correlation test in Sec. 4.2, it is suggested that (ENT, COR, CLU) is the best feature vector due to the better overall accuracies based on ENT and COR.

5. Conclusion

In this paper, wavelet transform and co-occurrence matrices were integrated to extract the co-occurrence features including angular second moment (ASM),

entropy (ENT), contrast (CON), homogeneity (HOM), dissimilarity (DIS), correlation (COR), and cluster tendency (CLU) for a description of pipe defects. The pipe defect of open joint on CCTV images was found to have the consistent textures due to large ASM and HOM values. On the contrary, most CCTV images of broken pipe display the complex textures because of the multiple sizes and shapes of debris.

A correlation test was implemented on the seven co-occurrence features to obtain an appropriate feature set for a further automated diagnosis of pipe defects. Based on the result of the correlation test (ASM, COR, CLU), (HOM, COR, CLU), and (ENT, COR, CLU) are considered as the candidate feature vectors due to low correlation coefficients (0.5). Moreover, COR was found to be rarely relevant to CLU. Finally, a discriminant analysis was processed to evaluate the discriminability of the pipe defects, and (ENT, COR, CLU) is the best feature vector according to a comparatively high discriminant accuracy. Consequently, the lower the correlation coefficients between the textural features are, the better the discriminability of pipe defects is.

References

1. M. D. Yang and T. C. Su, An automation model of sewerage rehabilitation planning, *Water Sci. Technol.* **54** (2006) 225–232.
2. C. Madryas and B. Przybyla, Inspection of pipes as an element of operating municipal sewerage networks, *Tunnelling Underground Space Technol.* **13** (1998) 57–64.
3. S. Cordes, K. Berns, M. Eberl, W. Ilg and R. Suna, Autonomous sewer inspection with a wheeled, multiarticulated robot, *Robot. Auton. Syst.* **21** (1997) 123–135.
4. R. Wirahadikusumah, D. M. Abraham, T. Iseley and R. K. Prasanth, Assessment technologies for sewer system rehabilitation, *Autom. Constr.* **7** (1998) 259–270.
5. J. M. Makar, Diagnostic techniques for sewer systems, *J. Infrastruct. Syst.* **5** (1999) 69–78.
6. O. Moselhi and T. Shehab-Eldeen, Automated detection of surface defects in water and sewer pipes, *Autom. Constr.* **8** (1999) 581–588.
7. R. A. Fenner, Approaches to sewer maintenance: A review, *Urban Water* **2** (2000) 343–356.
8. UK water industry engineering and operations committee, in *Sewerage Rehabilitation Manual*, Vol. II, 3rd edn. (Water Research Centre/Water Authorities Association, Swindon, UK, 1994), pp. 27–44.
9. R. A. Mckim and S. K. Sinha, Condition assessment of underground sewer pipes using a modified digital image processing paradigm, *Trenchless Technol. Res.* **14** (1999) 29–37.
10. K. Xu, A. R. Luxmoore and T. Davies, Sewer pipe deformation assessment by image analysis of video surveys, *Pattern Recogn.* **31** (1998) 169–180.
11. M. Acharyya and M. K. Kundu, Extraction of noise tolerant, gray-scale transform and rotation invariant features for texture segmentation using wavelet frames, *Int. J. Wavelets Multiresolut. Inf. Process.* **6** (2008) 391–417.
12. G. Sreelekha and P. S. Sathidevi, A wavelet-based perceptual image coder incorporating a new model for compression of color images, *Int. J. Wavelets Multiresolut. Inf. Process.* **7** (2009) 675–692.
13. V. Kabeer and N. K. Narayanan, Wavelet-based artificial light receptor model for human face recognition, *Int. J. Wavelets Multiresolut. Inf. Process.* **7** (2009) 617–627.

14. P. Wunsch and A. F. Laine, Wavelet descriptors for multiresolution recognition of handprinted characters, *Pattern Recogn.* **28** (1995) 1237–1249.
15. A. L. Amet, A. Ertuzun and A. Ercil, An efficient method for texture defect detection: Sub-band domain co-occurrence matrices, *Image Vis. Comput.* **18** (2000) 543–553.
16. B. K. Alsberg, A. M. Woodward and D. B. Kell, An introduction to wavelet transforms for chemometricians: A time-frequency approach, *Chemometrics Intelligent Laboratory Syst.* **37** (1997) 215–239.
17. R. C. Gonzalez and R. E. Woods, *Digital Image Processing*, 2nd edn. (Prentice-Hall, 2002).
18. W. Lu, X. Gao, D. Tao and X. Li, A wavelet-based image quality assessment method, *Int. J. Wavelets Multiresolut. Inf. Process.* **6** (2008) 541–551.
19. S. Arivazhagan and L. Ganesan, Texture segmentation using wavelet transform, *Pattern Recogn. Lett.* **24** (2003) 3197–3203.
20. B. Uma Shankar, S. K. Meher and A. Ghosh, Neuro-wavelet classifier for multispectral remote sensing images, *Int. J. Wavelets Multiresolut. Inf. Process.* **5** (2007) 589–611.
21. H. G. Li, Y. Li, C. P. Sun and X. L. Li, A new discrete wavelet transform fast algorithm with rational dilation factor, *Int. J. Wavelets Multiresolut. Inf. Process.* **6** (2008) 609–616.
22. B. H. Chen, X. Z. Wang, S. H. Yang and C. McGreavy, Application of wavelets and neural networks to diagnostic system development, 1, feature extraction, *Comput. Chem. Eng.* **23** (1999) 899–906.
23. M. K. Bashar, T. Matsumoto and N. Ohnishi, Wavelet transform-based locally orderless images for texture segmentation, *Pattern Recogn. Lett.* **24** (2003) 2633–2650.
24. H. G. Hwang, H. J. Choi, B. D. Kang, H. K. Yoon, H. C. Kim, S. K. Kim and H. K. Choi, in *Proc. the 7th International Workshop on Enterprise Networking and Computing in Healthcare Industry*, Busan, Korea (2005), pp. 345–349.
25. Z. Shang, Y. Y. Tang, B. Fang, J. Wen and Y. Z. Ong, Multiresolution signal decomposition and approximation based on support vector machines, *Int. J. Wavelets Multiresolut. Inf. Process.* **6** (2008) 593–607.
26. T. D. Chen, Licence-plate recognition using DWT and neural network, *Int. J. Wavelets Multiresolut. Inf. Process.* **4** (2006) 601–615.
27. R. Sanjeev Kunte and R. D. Sudhaker Samuel, Wavelet descriptors for recognition of basic symbols in printed Kannada text, *Int. J. Wavelets Multiresolut. Inf. Process.* **5** (2007) 351–367.
28. J. R. Parker, *Algorithms for Image Processing and Computer Vision* (Wiley, 1997).
29. G. Lohmann, Analysis and synthesis of textures: A co-occurrence-based approach, *Comput. Graph.* **19** (1995) 29–36.